



Shake table testing of a low damage steel building with asymmetric friction connections (AFC)

Ali A. Rad ^{a,*}, Gregory A. MacRae ^b, Nikoo K. Hazaveh ^c, Quincy Ma ^d

^a Aurecon New Zealand Limited, Engineering Consultant, Wellington 6011, New Zealand

^b University of Canterbury, Department of Civil and Natural Resources Engineering, Private Bag 4800, Christchurch 8140, New Zealand

^c WSP Opus, Engineering Consultant, Wellington 6011, New Zealand

^d The University of Auckland, Department of Civil & Environmental Engineering, Faculty of Engineering, Private Bag 92019, Auckland Mail Centre, Auckland 1142, New Zealand



ARTICLE INFO

Article history:

Received 1 July 2018

Received in revised form 15 December 2018

Accepted 17 December 2018

Available online xxxx

Keywords:

Shake table testing

Steel moment frame

Asymmetric friction connections

ABSTRACT

This paper describes the shaking table performance of a half-scale two-story steel moment frame with asymmetric friction connections (AFCs) at the column bases and at the beam ends. The dynamic properties of the test structure are determined using snap-back tests. The behavior of the test frame to ground motions was consistent with standard methods to estimate peak displacements, and residual displacements. When beam ends and the base-column joints were modelled by trilinear and bilinear hysteresis loops respectively, the response with time matched numerical simulations well. Residual drifts were <0.2% for peak inter-story drifts up to 3%, and <0.7% for peak inter-story drifts of 6.0% and the structure was able to manually restrained.

© 2019 Elsevier Ltd. All rights reserved.

1. Introduction

In light of recent major seismic events worldwide, it has become apparent that while modern design provisions ensure life safety in modern structures during severe earthquake events, structures may be damaged and require extensive repair or replacement. A recent research effort is to develop new solutions that will also minimize the possibility of structural damage. Such low-damage structures may be achieved by developing a behavior that is elastic, or by incorporating the use of energy dissipaters such as friction connections.

In friction connections, energy is dissipated as two surfaces slide against each other. The sliding resistance is determined by the clamping force provided by pre-tensioned high strength bolts and the friction coefficient between the sliding materials. Beam end friction connections for steel MRFs have been studied by Yang and Popov [1] where the researchers utilized symmetric friction connections (SFCs) in the top and bottom flanges of steel beams. The experimental test results showed a reliable frictional behavior with limited degradation. However, most realistic moment frames cannot deform in this manner since there is a slab on top of the beam. Connections which do not slide at the top flange have also been developed and tested [2–4]. These rotate about the top flange plate and sliding only occurs in the bottom flange plate thus minimizing interactions with the overlying floor slab and the effects of beam elongation as shown in Fig. 1.

In such connections the bottom flange of the beam is beside a plate extending from the column called the bottom flange plate. One shim is placed between the bottom-flange plate and beam. Another shim is placed between the bottom-flange plate and cap plate. When beam ends starts to rotate about the top flange plate, initial sliding occurs between the bottom-flange plate and beam. Later sliding occurs between the bottom-flange plate and cap plate. Since sliding does not initiate at both locations at the same time, it is referred to as an asymmetric friction connection.

Past studies of AFC were mostly experimental with AFCs applied to beam-to-column moment resisting joints [3,4], base-columns connections [5,8], Fig. 2a and braces [6,7], Fig. 2b. All of these configurations can possess good seismic performance. Also, a simple conceptual hysteretic behavior of beam end AFC connection was proposed. However, there are the following gaps in previous studies:

- No previous shaking table testing of an asymmetric friction connections structure is known to have been undertaken,
- Simple methods to estimate the peak and residual displacements of a realistic AFC frame have not been verified,
- Previous SHJ beam-column connection models, based on cyclic tests, assumed symmetric hysteresis models and ignored prying effects. These have not been compared with the overall performance of an physical AFC friction structure, and
- Structural resilience/reparability, which depends on the degree of damage, residual displacement, and ability to reinstate, has not been quantified for a realistic frame.

* Corresponding author.

E-mail: ali.rad@aurecongroup.com (A.A. Rad).

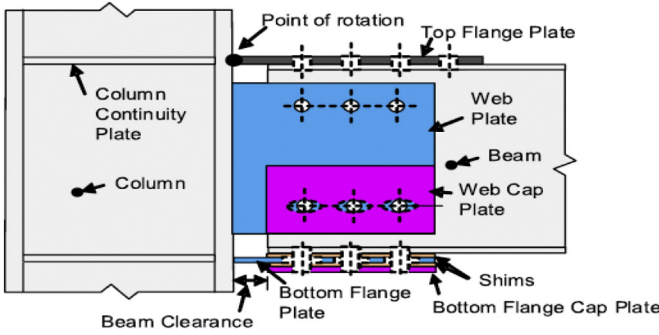


Fig. 1. Asymmetric friction connection (AFC) in beam column joint [4].

It is clear that there is a need to experimentally validate the seismic performance of whole AFC frame systems to develop further confidence amongst engineers for their adoption. This paper seeks to address this need by describing the shake table testing of a half-scale steel frame building with AFCs at the column bases and beam ends. In particular, answers are sought to the following questions:

1. How do these beam and column friction connections behave during excitation?
2. What is the peak and residual response for this particular structure?
3. Can numerical modelling predict the experimental performance?
4. Can beam and column AFCs be considered “low damage”?

2. Literature review

Idealised hysteretic behaviour of beam-end AFC connections, known as sliding hinge joints (SHJs), was described by MacRae et al. [4]. It was defined over 5 different stages as shown in Fig. 3 beginning with (a) before sliding, where beam flexure dominates the response before there is sliding in the connection; (b) initial sliding, where sliding occurs between the bottom of the beam flange and the bottom flange plate. At this stage the bottom flange cap plate is not sliding because the shear force imposed on it is relatively small. Stage (c) cap plate sliding occurs as the shear force and deformations become greater. Stage (d) reverse loading first sliding occurs between the bottom of the beam flange and the bottom flange plate and finally stage (e) occurs at larger displacements in the opposite direction. Sliding on both surfaces causes approximately twice the resistance from one surface.

However, in this model the prying effect of the bottom flange plate was not explicitly considered. Also, the sliding force for reverse loading, Stages (d) and (e), were considered to have same magnitude at Stages (b) and (c) respectively. Furthermore, the experimental studies by Clifton [3] showed that the idealised model did not match the experimental behaviour well.

The nominal sliding force at each AFC bolt location, F_s , is given as $F_s = \mu \times \eta \times N_{tf}$, where μ is the effective friction coefficient, η is the number

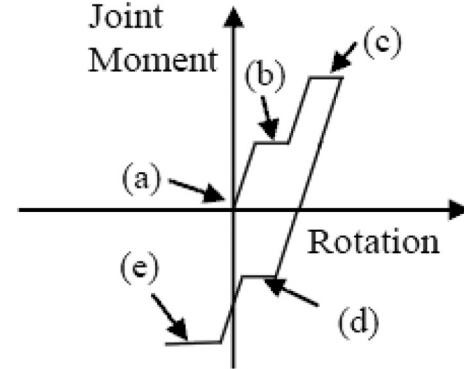


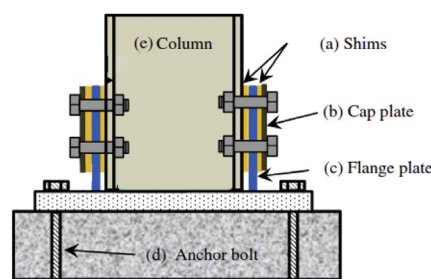
Fig. 3. Hysteretic behaviour of asymmetric friction connection (AFC) at beam end [4].

of shear planes ($= 2$, for both surface sliding), and N_{tf} is the proof load per bolt. The median effective friction coefficient of steel against high hardness Bisalloy 500 (shims in an AFC connection) is equal to 0.21 according to Chanchí et al. [6].

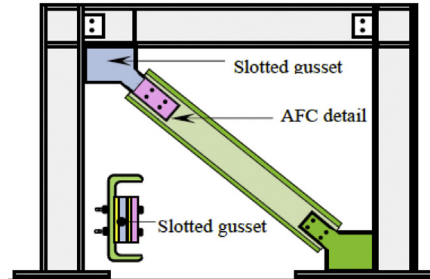
Column base AFC hysteretic behaviour has been studied by Bourzouie et al. [5]. The column base AFC could be modelled by a bilinear hysteresis loop. Sliding, prying, and axial force were three mechanisms providing moment resisting in the base connection as shown in Fig. 4. Based on this the maximum base moment from lateral loading causing strong-axis bending, M_{Tot} , was calculated by Eq. (1) where M_{Slide} is the moment resulting from sliding friction, M_{Prying} is the elastic-prying moment mainly from flange plate bending on the compression side of the column, and M_{Axial} is the moment from axial force. In the equation, n_{Bolt} is the number of the bolts in each AFC, F_s is the sliding force for each bolt as defined in Eq. (5), θ_{Base} is the base rotation, H_{fp} is the distance from the top of the flange plate to the base plate, I_{fp} is the second moment of area about the weak axis of the flange plate, d is the distance from the sliding bolts to the neutral axis, and D_{Axial} is the perpendicular distance from the centre of axial force to the neutral axis.

$$M_{Tot} = M_{Slide} + M_{Prying} + M_{Axial} = (n_{Bolt} \times F_s \times d) + \left(\frac{\theta_{Base} \times 3EI_{fp}}{H_{fp}} \right) + (P \times D_{Axial}) \quad (1)$$

Residual displacement prediction methods have been developed by MacRae and Kawashima [9] for elastoplastic single-degree-of-freedom (SDOF) oscillators with specified ductilities of 2, 4 and 6, post elastic stiffness ratios ranging from 0.25 to 1 and fundamental periods from 0 to 3 s. It was shown that the ratio of the residual displacement to the maximum possible residual displacement is almost totally dependent on the post-elastic stiffness ratio, r , of the force-displacement hysteretic curve and ductility demand, μ . The oscillators with positive stiffness ratios generally have small residual displacements, while those with negative stiffness ratios have larger residual displacements. The residual displacement, D_r , was calculated by Eq. (2) where D_{mr} is the maximum



(a) Base column joint [5]



(b) Braces [6]

Fig. 2. Asymmetric friction connection (AFC) in base column and braces.

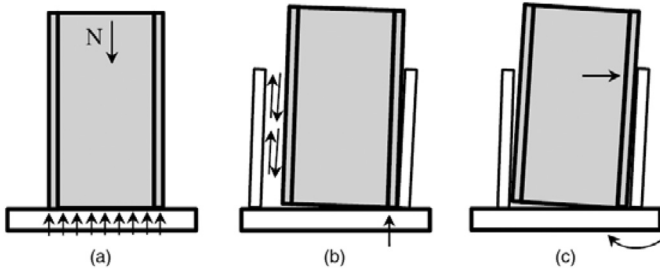


Fig. 4. Mechanisms of load transfer at the base column: (a) axial force; (b) sliding; (c) prying [5].

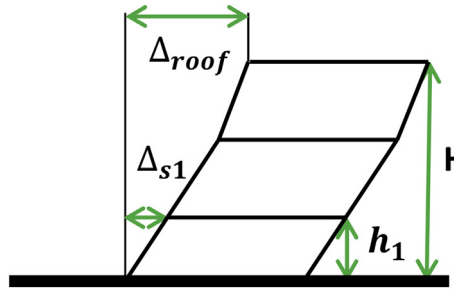


Fig. 5. DCF Definition.

possible residual displacement based on slow unloading from the peak displacement and D_{rr} is a non-dimensional residual displacement ratio which has values ranging from zero to unity. A graph of D_{rr} for different ductility, μ , and r , have been obtained in MacRae and Kawashima [9]. D_{mr} was calculated by Eq. (3) where D_y is the yield displacement.

$$D_r = D_{rr} \times D_{mr} \quad (2)$$

$$D_{mr} = \begin{cases} (\mu-1)(1-r)D_y & r(\mu-1) < 1 \\ \frac{(1-r)}{r}D_y & r(\mu-1) \geq 1 \end{cases} \quad (3)$$

Peak interstory drifts can be estimated according to methods of MacRae et al. [10]. They showed that if the structure deforms with a linear distribution of displacements and columns are continuous over several stories of a structure, then the stiffness of the columns will limit the possible drift concentration. This is known as the “continuous column

concept” and it emphasizes the continuous column stiffness. The drift concentration factor (DCF), is defined by Eq. (4) and Fig. 5 where the roof drift, δ_{roof} , is simply the roof displacement, Δ_{roof} , divided by the height of the roof from the ground, H , and the story drift, δ_s , is the maximum value of interstory displacement, Δ_{si} , divided by story height, h_i , for all stories, i , as shown in Eq. (5). If the columns are very stiff, then the structure is moves over linearly, there is no drift concentration, and the DCF is unity. Otherwise, DCF is greater than unity.

$$DCF = \frac{\delta_s}{\delta_{roof}} \quad (4)$$

$$\delta_s = \max_i \left\{ \frac{\Delta_{si}}{h_i} \right\} \quad (5)$$

3. Test specimen design

The two storey test specimen was designed as a full-scale prototype building according to the Equivalent Static Method in NZS1170.5 [11]. The structure was assumed to be located in Wellington, with $Z = 0.4$ and soil type C. It was designed assuming beam end and base column connections were fixed. Assuming rigid and strong connections the design ductility was unity and the design drift in the Design Level (DL) earthquake event (1-in-500 year earthquake shaking) was 2.0%. AFC connections at the column bases and beam ends were then designed to have drifts corresponding to design ductilities, μ , of 3 and 6 respectively. Capacity design considerations were checked to ensure that the beams and columns remained elastic during both design level (DL) and maximum considered events (MCE). The MCE shaking had a probability of exceedance of 1/2500 years. The test specimen is composed of two parallel steel frames (which are yellow in Fig. 6) with AFC connections at the base column and beam ends. The beam end AFC shown in Fig. 7a is designed to rotate about the top flange plate and slide only on the bottom flange plate. The moment is carried by friction between plates as no web plate exists. The friction plates are designed with sufficient tension capacity to carry the plastic moment capacity of the beam section ($M_n = F_y \times S = 24 \text{ kN.m}$ where S is the plastic section modulus and F_y is the minimum specified yield stress for the steel grade) and capacity design requirements based on frictional sliding were checked. These involved an overstrength factor of 1.4 [12]. The nut-rotation method with half a turn after snug tightening according to NZS3404 [13] was used for tightening 4 M12 Grade 8.8 bolts in the AFCs to their proof load (45kN). At the base connection, the moment is carried by friction. Axial force is

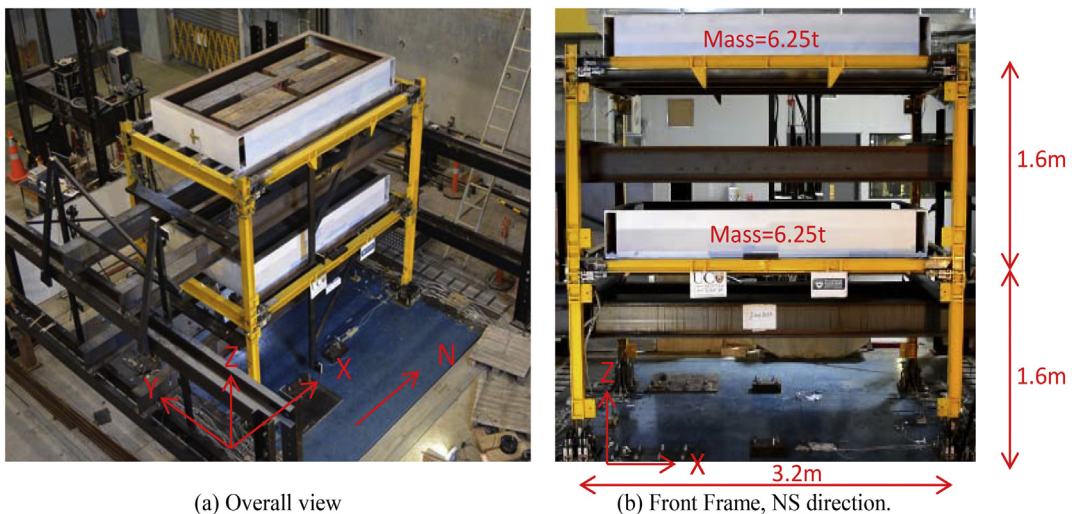


Fig. 6. Test building views.

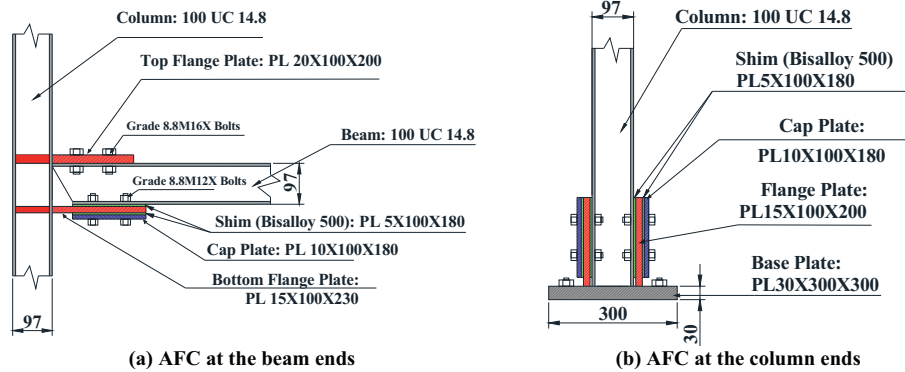


Fig. 7. AFC details (All units mm).

transferred directly by the column to the base plate as shown in Fig. 7b. In the transverse direction, the two frames are joined by short transverse beams. The lengths of beams and columns, and the amount of the total mass at each floor, are provided in Table 1. The black beams under the yellow frame are part of a catch frame to provide safety during tests. The white channels on top of the yellow beams form a tray into which steel is placed to increase the mass at that level Fig. 8.

Beam top/bottom flange plates, and the column flange plates, were connected to the beams and columns respectively with full penetration SP (structural purpose) butt welds applied in the steel fabrication shop. A W50X wire type electrode was used with a nominal tensile strength of 480 MPa so any inelastic deformation was expected to occur in the plates rather than in the welds. Furthermore, Khoo et al. [14] has shown that low cycle fatigue fracture due to plate axial, flexural and shear strains, is not likely to occur even after several strong shaking events.

The prototype was scaled to meet the requirements of the shake table. Considering the limitations of the shake table, as well as the added artificial mass, the three fundamental scaling factors (SF) specified were α_l for length, α_m for mass, and α_s for stress. These were set to 0.5, 0.25 and 1, respectively. Thereafter, other SFs such as time, acceleration, force were calculated based on the above three factors as shown the relationship in Table 2. In Table 2, the similitude relationships for key quantities often considered in structural engineering are presented. Here, the 'subscript' M refers to the model and symbol P refers to the prototype.

4. Instrumentation

Test frame instrumentation consisted of a combination of string pots, accelerometers, strain gauges, potentiometers, and load cells, as shown in Fig. 9. The relative displacement of each story, along with the location of each string pot allowed for the determination of the inter-storey drifts. They were attached between the columns and a fixed reference frame as shown in Fig. 9. The string pots had a maximum displacement of 1000 mm in each direction from the resting position and a resolution of 0.0001 m. The local behaviour of the beam-column connections and column base connections were recorded by two and four parallel potentiometers respectively. These were placed across each connection interface (Fig. 9). The neutral axis and rotation of the

connection are subsequently estimated by interpolation assuming a linear strain profile across connections. Six horizontal accelerometers (two at each floor level (both sides) and two on each side of the shake table) were placed on the structure in the direction of loading as shown in Fig. 9. Strain gauges were also attached at beam and column ends before sliding plates on both top and bottom sides of the sections to measure the strain and moment force at each connection.

Donut load cells (LWO-30, Transducer Techniques Company) were placed between bolt heads and the plates to measure bolt tension during plate sliding as shown in Fig. 10. All load cells were calibrated before installing in the connections. Their accuracy was checked by applying compression force and monitoring the load cell readings. The load cells were sandwiched between two Grade 350 steel washers to maximize load cell reading accuracy. The nut rotation method, with half a turn after snug tightening according to NZS3404 [13], was used to tighten bolts. This resulted in a bolt tension force of 45 to 50 kN. This is greater than the proof load of 45kN as expected.

5. Test protocols

A set of 6 earthquake ground motions selected from both NZ local earthquake events [15] and the NGA database [16] are listed in Table 3. The time-step of each ground motion was reduced by a factor of 0.7 to fulfil similitude requirements in Table 2 and to ensure similar peak accelerations in the model and prototype. Fig. 11 compares the NZ code [11] spectra with the spectral acceleration of the ground motions.

6. Shake table response

6.1. Test model dynamic characteristics

Snap-back (free vibration) tests were performed on the test structure to determine the natural period and damping ratio of the structural system before the shake table excitations were applied. The top floor of the model was pulled from both sides to a displacement of about 3 mm, then it was released. Fig. 12 shows the fundamental period of the structure which was found to be 0.47 s. The damping ratio was calculated by the logarithmic decrement method in Eq. (6) was 3.4%.

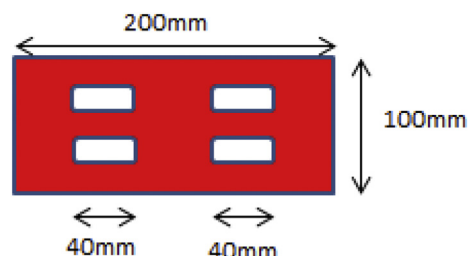


Fig. 8. Flange plate detail.

Table 1
Properties of the test building.

Items	Properties
Inter-story height [m]	1.6
Bay length [m]	3.2
Building width [m]	2
Mass per floor [ton]	6.25
Column section	100 UC 14.8 Grade 320
Beam section	100 UC 14.8 Grade 320

Table 2
Similitude Relationships.

Quantity	Symbol	Relationship	Parameter	Similitude
Length	α_l	Specified	0.5	$L_M = 0.5 L_p$
Mass	α_m	Specified	0.25	$m_M = 0.25 m_p$
Stress	α_s	Specified	1.0	$S_M = S_p$
Area	α_A	α_l^2	0.25	$A_M = 0.25 A_p$
Time	α_t	$\sqrt{(\alpha_m/(\alpha_s \alpha_l))}$	0.7	$t_M = 0.7 t_p$
Velocity	α_v	α_l/α_t	0.7	$v_M = 0.7 v_p$
Acceleration	α_a	$\alpha_l/\alpha^2 t$	1	$a_M = a_p$
Force	α_f	$\alpha_m \alpha_a$	0.25	$F_M = 0.25 F_p$
Moment	α_M	$\alpha_f \alpha_l$	0.125	$M_M = 0.125 M_p$
Strain	α_e	α_s	1	$\varepsilon_M = \varepsilon_p$

Torsional displacements of the frame were negligible (<0.1% of the peak displacements).

$$\xi = \log\left(\frac{A_0}{A_1}\right)/2\pi \quad (6)$$

6.2. Structure response to earthquake records

6.2.1. Peak displacement response

Fig. 13 shows the structure peak roof displacement response with spectral displacement at a fundamental period of $T = 0.47$ s for different ground motion records with scale factors, α_a , of 50%, 75% and 100%. For

most records with low intensity levels ($\alpha_a=50\%$), the spectral displacements of the records was close to, but generally less than, the peak displacement of the structure. Also, with increasing ground motion intensity the peak roof displacement of the structure increases relative to the spectral displacement of the records. Possible reasons for this include: (i) the multi-storey structure mass centroid is below the roof level; (ii) higher mode effects occur; (iii) the structure has non-linear behaviour which is likely to be bigger than the elastic response especially for short period structures.

6.2.2. Base shear response

Floor design forces at any time were obtained by multiplying the floor accelerations by the floor mass. The building base shear at any time was obtained by summing these together. Fig. 14 shows some base shear vs. roof displacement plots under different ground motions. The experimental data is roughly consistent with that from analysis of a single degree of freedom system with a bi-linear hysteresis loop and a post-elastic stiffness factor, r , of about 0.3 as shown by the red lines.

6.2.3. Peak and residual drift response

Fig. 15 shows the peak and residual drift responses over the structure height under different ground motion records and with different intensity levels. The frame was manually returned to its initial vertical position, and new bolts were inserted and tightened before each run. The number shown after “Residual and Peak Drift” is the record acceleration scale factor considered. Peak drifts are generally similar at both

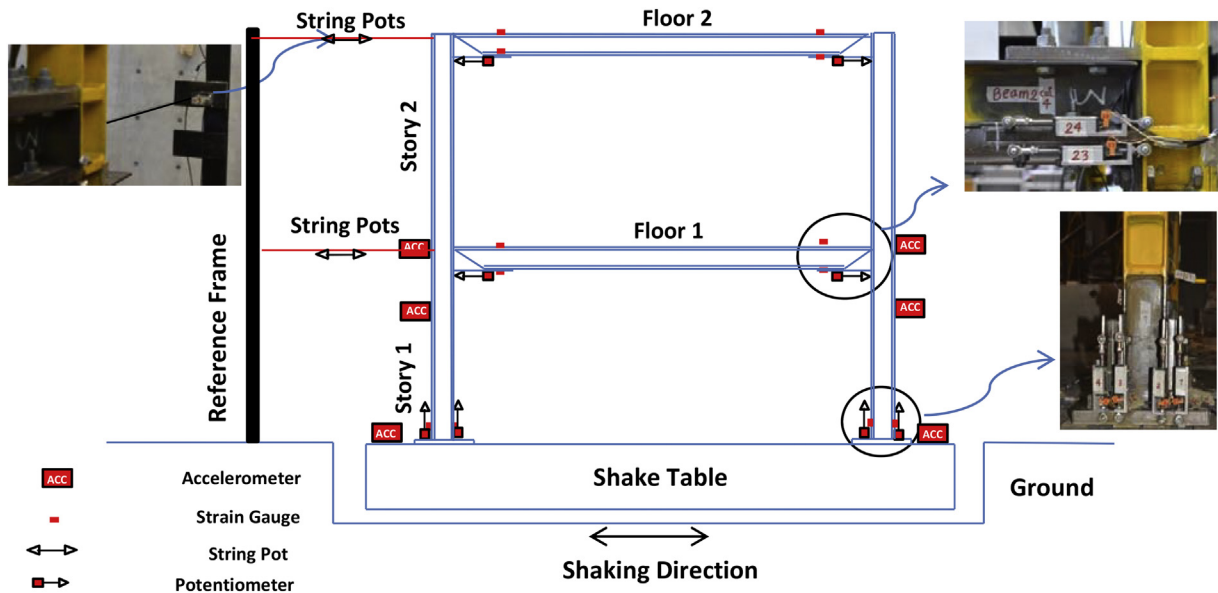


Fig. 9. Instrumentation arrangement.

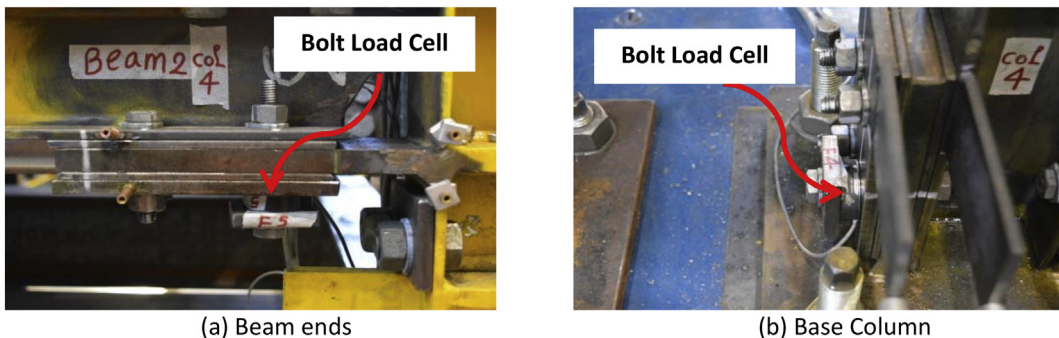


Fig. 10. Bolt load cells.

Table 3
Ground motions (Unscaled properties).

No	EQ name	Station	Orientation	Date	M _w	PGA (g)	PGV (mm/s)	PGD(mm)
1	Christchurch, NZ	CCCC	N-S	22/02/2011 12:51 pm	6.2	0.49	480	100.8
2	Christchurch, NZ	REHS	N-S	22/02/2011 12:51 pm	6.2	0.71	587	143.8
3	Northridge, US	Sylmar	N-S	1994	6.7	1.02	467.6	110.9
4	Kobe, Japan	KJM	N-S	1995	6.9	0.82	569.1	86.7
5	Tabas, Iran	Tabas	N-S	1978	7.4	0.85	694.5	175.7
6	Bam, Iran	Bam	N-S	2003	6.6	0.81	868.84	166.7

floor levels. Often these occur at similar times indicating that the structure moves with an almost linear pattern with little drift concentration (i.e. the DCF is close to unity) as shown in Table 4 computed using Eq. (4). Up to a peak drift response of 3% the residual drift response was not >0.2%. For a peak drift response of 6.0%, the residual drift response is 0.7%.

Residual drift is also calculated by Eqs. (2) and (3). Here the ductility, μ , post elastic stiffness ratio, r , and yield displacement, D_y , are calculated from Fig. 14 where the maximum peak displacement, D_{max} , is about 150 mm, the yield displacement, D_y , is about 25 mm, so the ductility, $\mu = D_{max}/D_y = 150/25 = 6$; and post elastic stiffness ratio is 0.3. According to Eq. (3) D_{mr} is 58.5 mm, D_r is 0.25 for a ductility of 6 from Fig. 6 of MacRae and Kawashima [9] and the average residual displacement, D_r , is 14.6 mm from Eq. (2). Moreover, to calculate the drift, the equivalent height of the SDOF substitute structure, H_e , is considered to be at the structure centre of mass which is 2.4 m above the ground level. Therefore, the computed residual drift demand, $\delta_r = Dr/H_e = 14.6\text{mm}/2400\text{mm} = 0.6\%$. This value is consistent with that obtained from the shake table tests shown in Table 4 which ranges from 0% to 0.72%.

6.2.4. Asymmetric friction connection (AFC) behaviour

Fig. 16 shows the moment-rotation relationship at the beam end (1st floor, front frame, north end, previously shown in the Fig. 6) during different earthquake records. In addition, a red line is provided which seems to follow the behaviour of the largest displacement cycle firstly in the positive direction then in the negative direction. It is defined empirically based on the observed response to the Bam record in Fig. 16a where there is almost monotonic behaviour initially. For the other records, the first line (o to a) and second line (a to b) have the same strength increase. The third line (b to c) is extended to the peak positive displacement and unloading on the 4th line (c to d) has the same

magnitude and slope as the initial (o to a) line. The 5th line (d to e) has same slope as (a to b), but the magnitude of point (e) is dependent on the magnitude at point (c) which is explained below. The last line (e to f) has the same slope as (a to b) and is extended to the peak negative displacement.

The AFC hysteretic behaviour can be defined by the points up to (f). Point (a) sliding initiates between the bottom flange plate and beam flange, and at Point (b) sliding initiates between the cap plate and beam flange. In both stages flange plate prying occurs. Because of the prying effect, the lines between point (a) and (b) and also between (b) and (c) are not flat but are inclined. This prying increases the moment resistance. When the moment resistance due to the prying effect in the end beam connection, M_{Prying} , is assumed to be that from only the beam compression side flange plate bending it may be computed based as $M_{Prying} = \left(\frac{\theta_{base} \times 3EI_p}{H_{fp}}\right)$ based on Eq. (1). This was not explicitly considered in the model described by MacRae et al. [4] for beam-end AFCs as shown in Fig. 3 and it is probably more significant in this case with small members and relatively thick plates. The moment resistance at Points (a) and (b), ($M_a = 3\text{kN.m}$ and $M_b = 7\text{kN.m}$) are the same for all records. At Point (c), the moment resistance at the maximum positive rotation, M_c , depends on record used. For example, $M_c \approx 10\text{kN.m}$ for the Bam record. Points (d) and (e) occur during reverse loading. First, initial sliding occurs between the bottom of the beam flange and the bottom flange plate (d to e). At larger reverse loading displacements, sliding of cap plate occurs from e. Point (e) does not occur at the same absolute moment resistance as Point (b). This is different from the model described by MacRae et al. [4] for the beam end AFC where the sliding occurs with the same absolute moment in each direction as shown in Fig. 3 where prying was ignored.

After Point (c), unloading and the loading in the reverse direction occurs. The amount of unloading and loading moment force before initial sliding in the reverse direction is $2M_a$. Therefore, the moment at Point (d), M_d , equals $M_c - 2M_a$. Also, the moment force at Point (e), M_e , equals $M_c - 2M_b$. For example for Bam records, M_d equals $4\text{kN.m} (= 10\text{kNm} - 2$

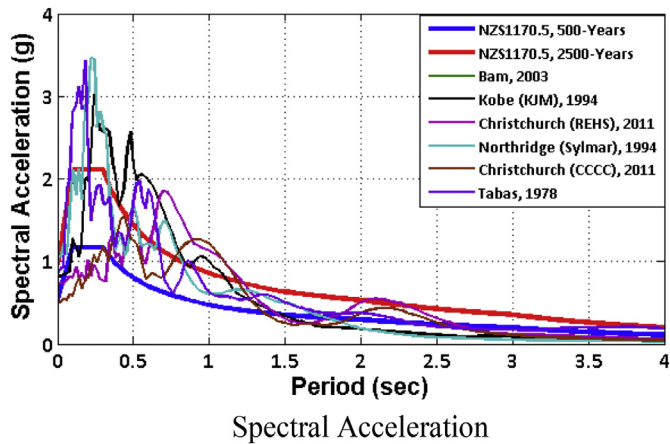


Fig. 11. Spectral acceleration of ground motions compared with NZ code spectra [11]. (3.4% damping, $Z = 0.4$, Soil C, $S_p = 1.0$, Time scale = 0.7)

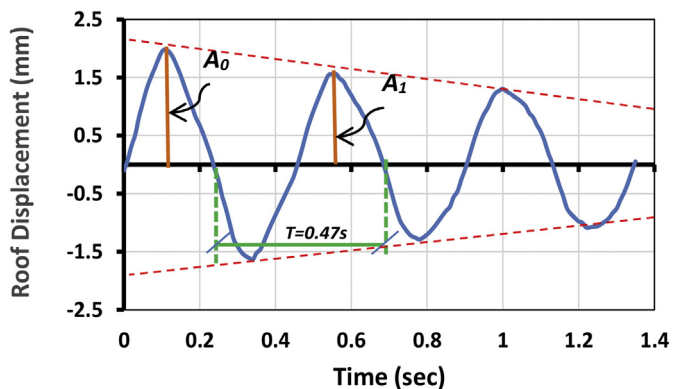


Fig. 12. Free vibration response.

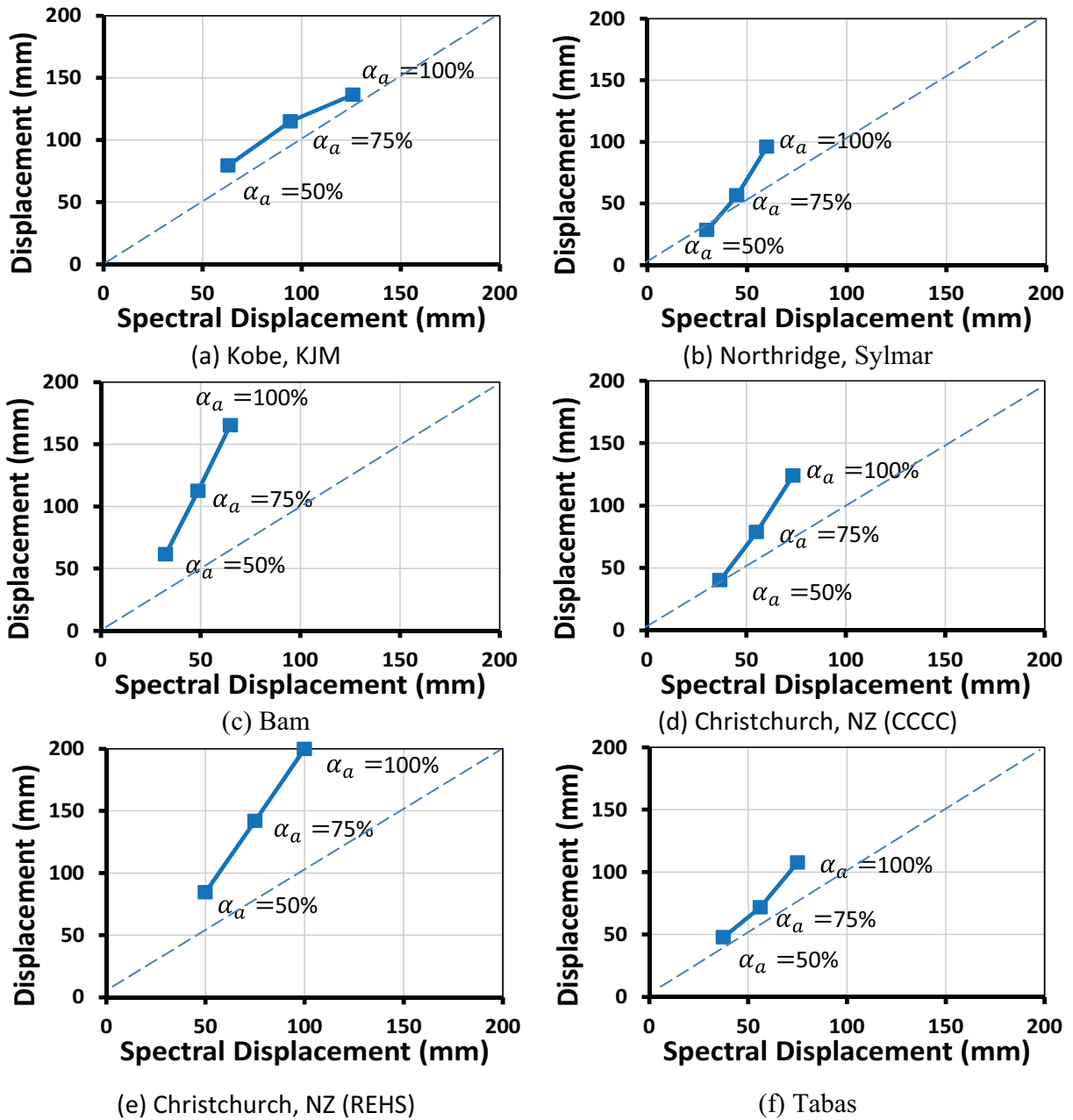


Fig. 13. Roof displacement variation with spectral displacement.

$\times 3\text{kNm}$) and M_e equals -4kNm ($= 10\text{kNm} - 2 \times 7\text{kNm} = -4\text{kNm}$). The horizontal dashed purple lines in Fig. 16 shows the sliding moment associated with first and second sliding at the beam ends at Points (a) and (b). Also, horizontal dashed green lines show the sliding moment associated with first and second sliding in the reverse loading at the beam ends at Points (d) and (e).

The bottom flanges force when the second stage of sliding initiates (Point b) can be calculated as the moment divided by the distance between the flange plate centres, $M/(d + t_{fp}) = 7\text{kNm}/0.102\text{ m} = 67\text{ kN}$. The effective friction coefficient, μ , computed as the flange sliding force divided by the sum of the bolt proof loads divided by the number of interfaces [4], for the M12 Grade 8.8 structural bolts is $67\text{kN}/(45\text{kN}/\text{bolt} \times 4\text{bolts} \times 2\text{interfaces}) = 0.19$ where 45kN is the proof load. This is close to the value recommended for design of 0.21 associated with sliding on both surfaces and it is greater than the minimum dependable

value of $\phi 0.21 = 0.7 \times 0.21 = 0.15$ [4]. The peak moment of 12 kN.m obtained is associated with an effective friction coefficient of 0.28, which is close to the overstrength value recommended for design of $\phi 0.21 = 1.4 \times 0.21 = 0.30$ [12], even though prying effects are significant for this particular connection.

Fig. 17a and b show the hysteretic behaviour of the AFC at the 1st floor, front frame, north beam end (previously shown in Fig. 6) subject to the Christchurch (CCCC) record with 50% and 100% acceleration scales. The beam end AFC hysteretic behaviour for 100% scale shaking is approximately tri-linear relationship, while for lower shaking levels, only the first 2 stages of this relationship (i.e. a bi-linear relationship) are needed to describe the behaviour. It is because the two friction surfaces in the connection do not start to slide at the same time as shown in Fig. 18. It is only at large displacements that sliding of cap plate occurs. In these tests the cap plate started to slide when the relative beam to

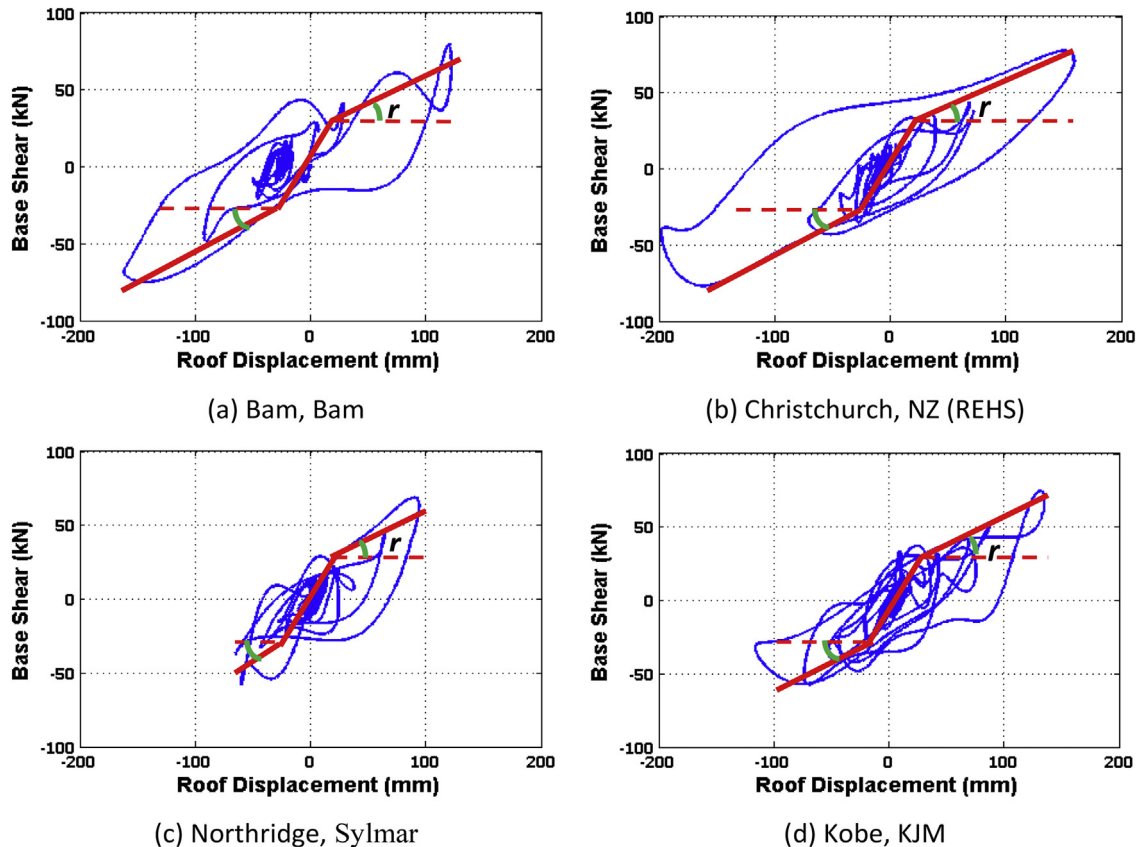


Fig. 14. Roof displacement vs base shear.

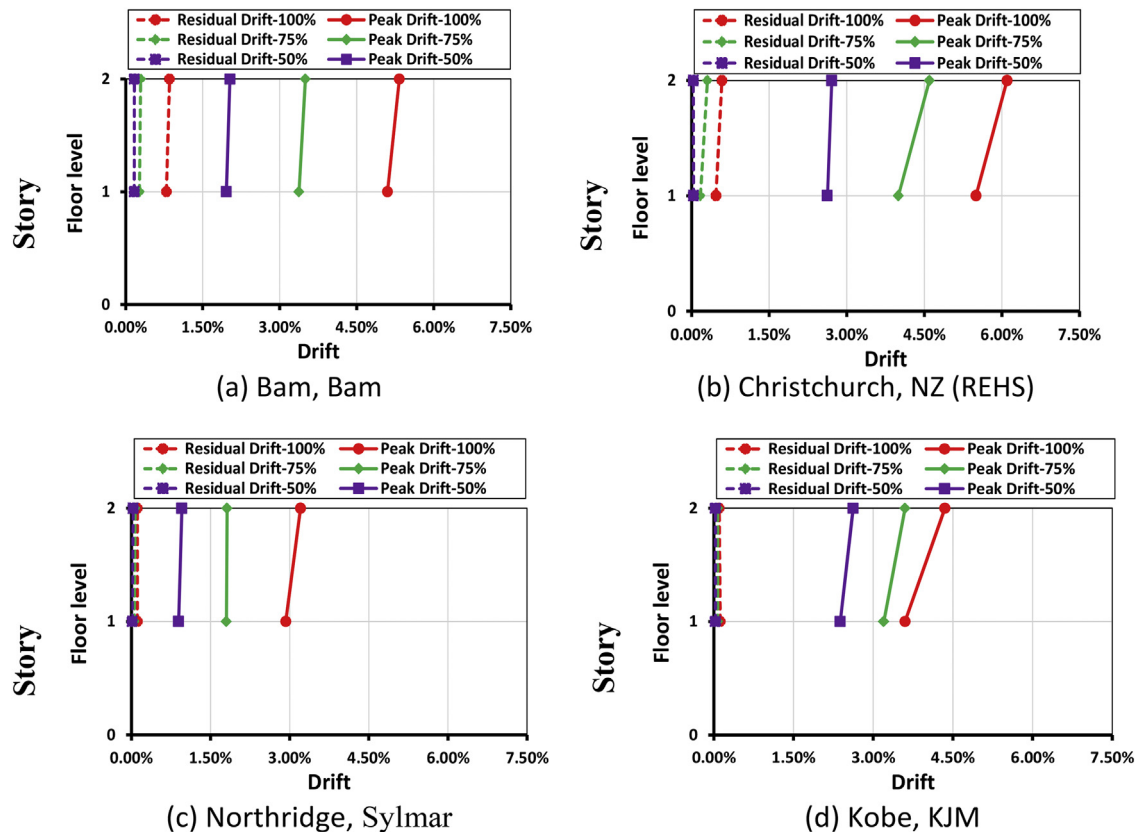


Fig. 15. Peak and residual story drift response.

Table 4

Experimental drift concentration factor, DCF , at 100% of each record.

EQ	Max. roof drift	Max. interstory drift ratio	Max residual drift ratio	DCF at peak drift
Bam, Iran	5.31%	5.20%	0.72	0.98
Northridge (Sylmar)	3.13%	3.21%	0.11	1.03
Christchurch (REHS)	6.25%	6.10%	0.59	0.98
Kobe (KJM), Japan	4.38%	4.35%	0	0.99

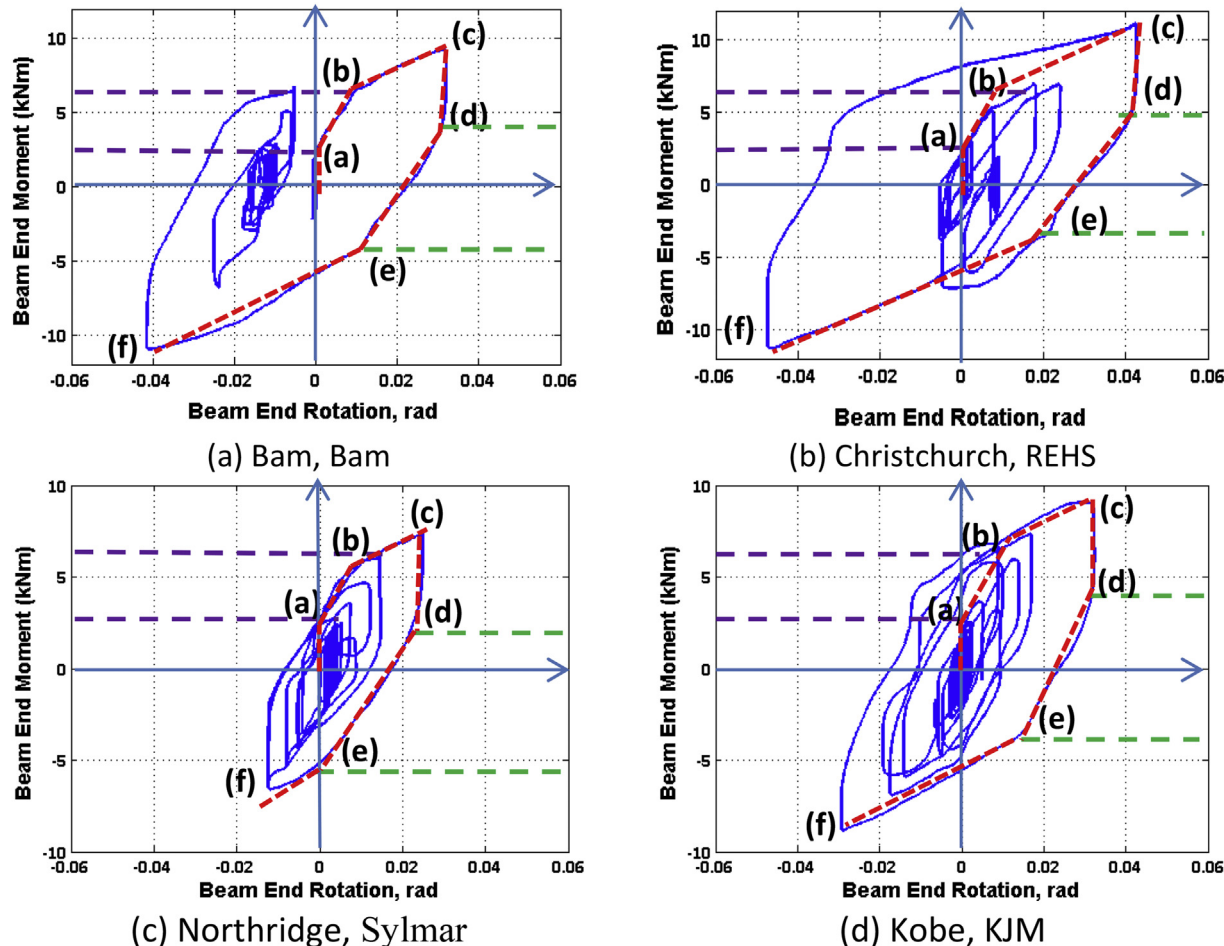


Fig. 16. Beam end AFC hysteretic behaviour, Acc. scale of 1.0.

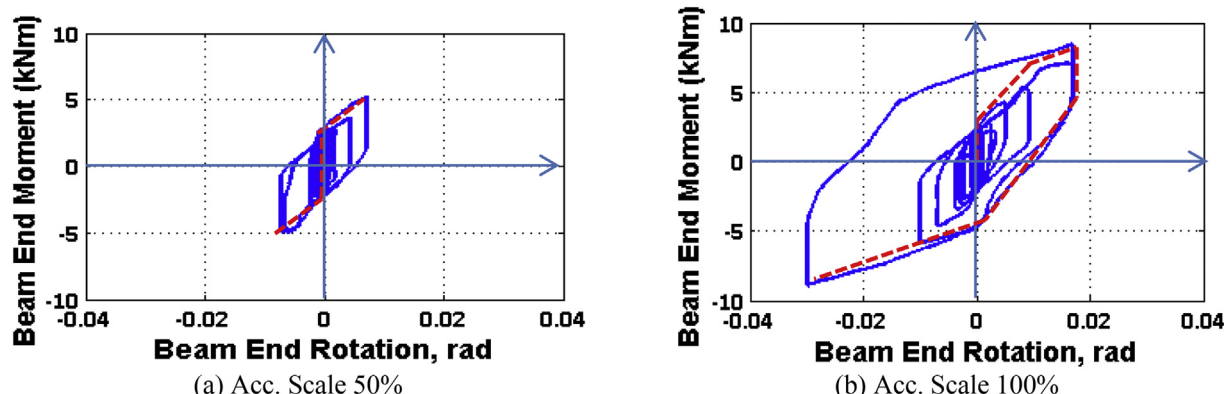


Fig. 17. Hysteretic behaviour of AFC at beam end under Christchurch (CCCC) record.

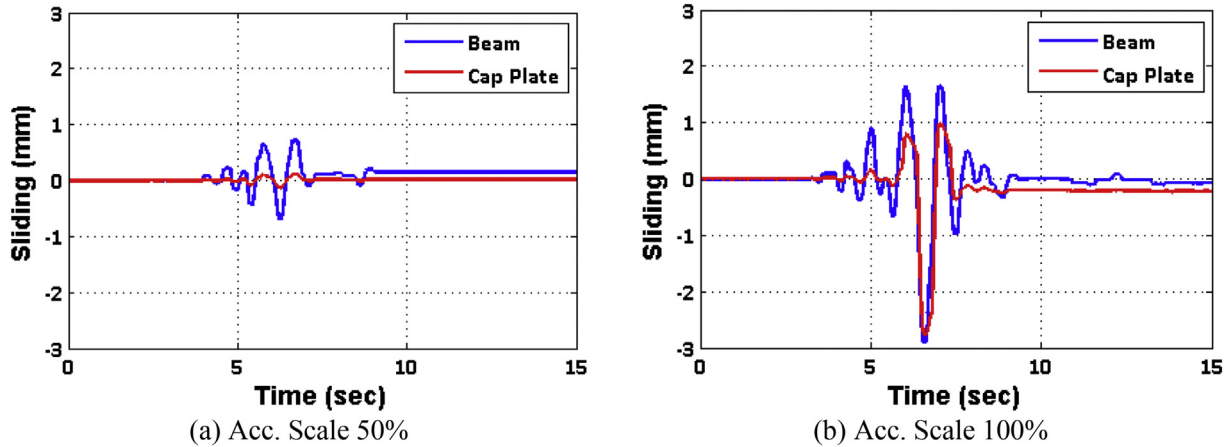


Fig. 18. Beam and cap plate sliding relative to slotted plate vs time (CCCC record).

column flange plate sliding displacement is about 1 mm. This is associated with a beam rotation of about 1.0% as shown in Fig. 18.

Fig. 19 shows the hysteretic behaviour of the AFC at a base column joint (shown in the Fig. 6, north end, front frame). In addition, a red line is provided to approximate the envelope behaviour. It is used to represent key feature of behaviour especially for a largest displacement

cycle behaviour. This bilinear behaviour with a high initial rotation sliding stiffness is consistent with by the work on base connections by Bourzouie et al. [5].

The base connection moment results from three components, (i) the moment from axial force (M_{Axial}), (ii) the moment resulting from sliding friction (M_{Slide}), and (iii) the elastic-prying moment (M_{Prying}).

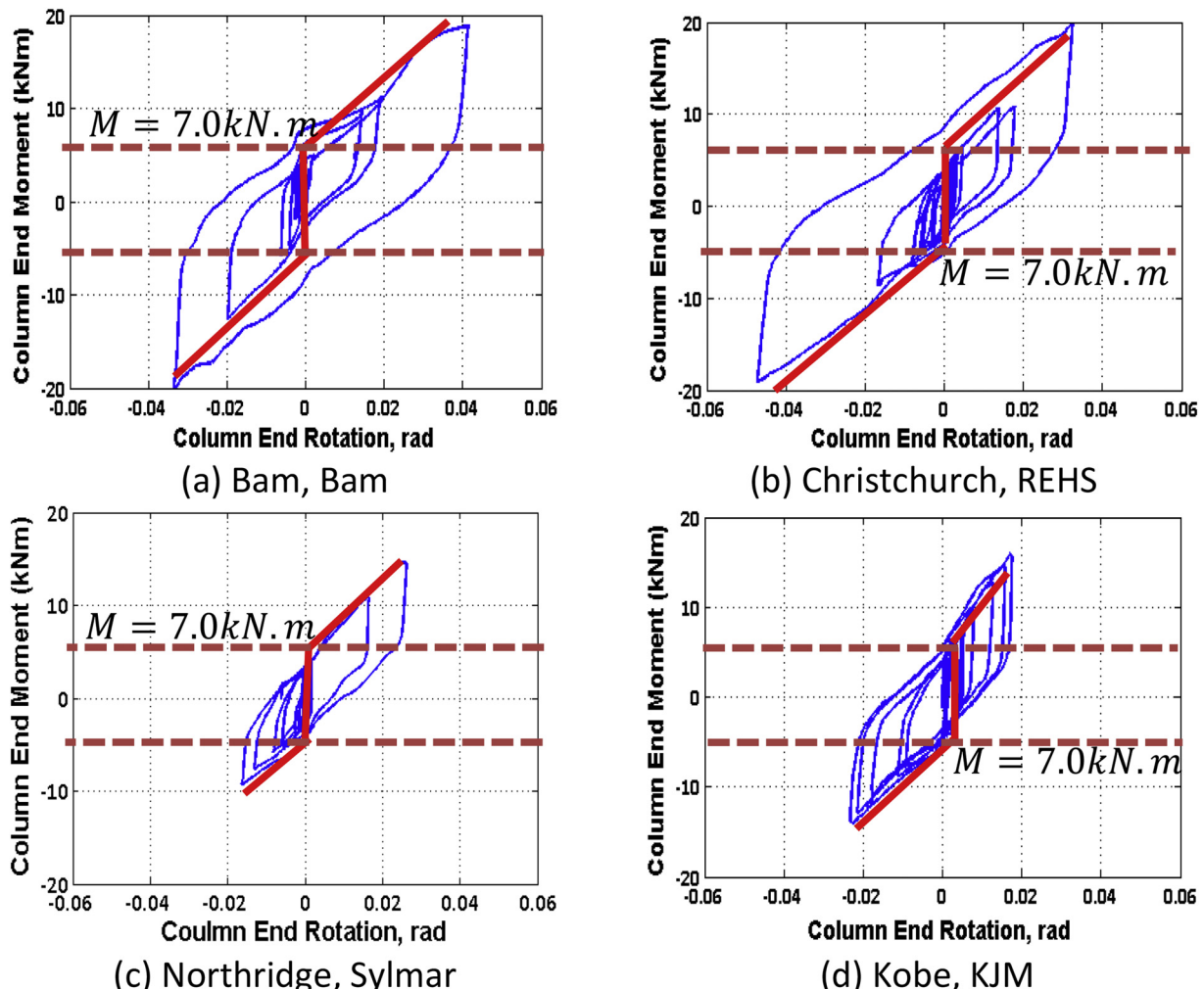


Fig. 19. Hysteretic behaviour of AFC at column base under different ground motions, Acc. Scale of 1.0.

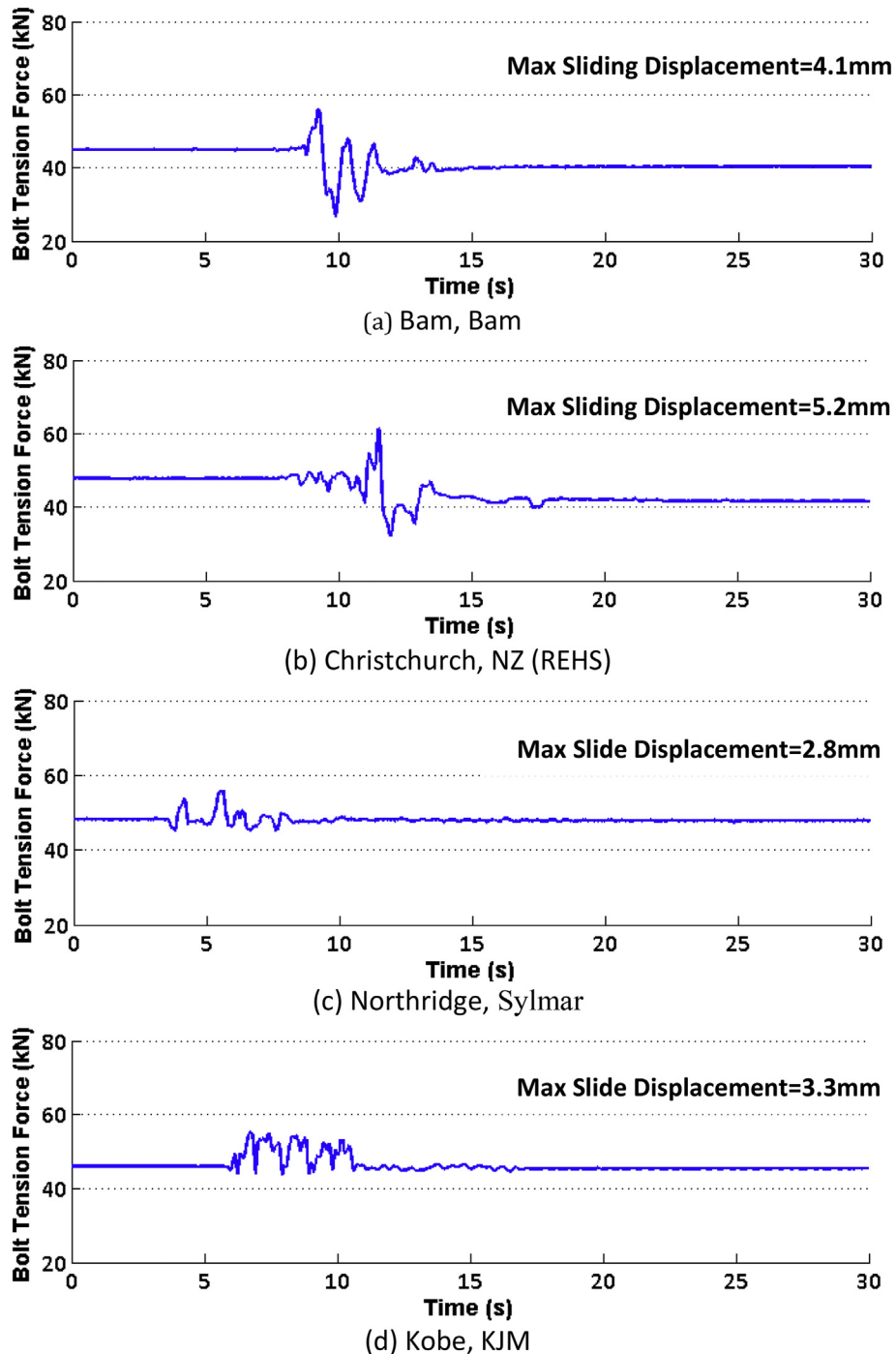


Fig. 20. Changing of tension force of the bolts during sliding under different ground motions.

The initial column base AFC sliding occurred at a column moment of about 7kN.m. At this stage, the moment resistant results of only M_{Axial} , and M_{Slide} and there is not much prying moment because of small amount of rotation. Based on Eq. (1), M_{Axial} is $P \times D_{Axial} = 50 \times 50 = 2.5\text{kN.m}$ where D_{Axial} is the perpendicular distance from the centre of axial force to the neutral axis and, P , is the peak axial force. The remainder of the moment resistance is due to frictional sliding where M_{Slide} equals 4.5kN.m.

After initial sliding, the prying effect also increases the column moment demand. For example, at a rotation of 1.5%, the column moment

is about 10.0kN.m. Here, 2.5kN.m (25%) of this amount is due to the axial force (M_{Axial}), 4.5kN.m (45%) is because of friction (M_{Slide}), and 3.0kN.m (30%) is due to the prying effect (M_{Prying}). After 2% column base rotation, the cap plate sliding also occurs. At larger rotations, all moment increase is due to prying alone.

The sliding frictional force can be calculated as the friction moment divided by the distance between point of rotation and sliding surface, $M/(d + t_{fp}) = 4.5\text{kNm}/0.105\text{ mm} = 42\text{kN}$. The effective friction coefficient at initial sliding using Eq.(1), after considering the effect of axial force, is computed as the flange sliding force divided by the

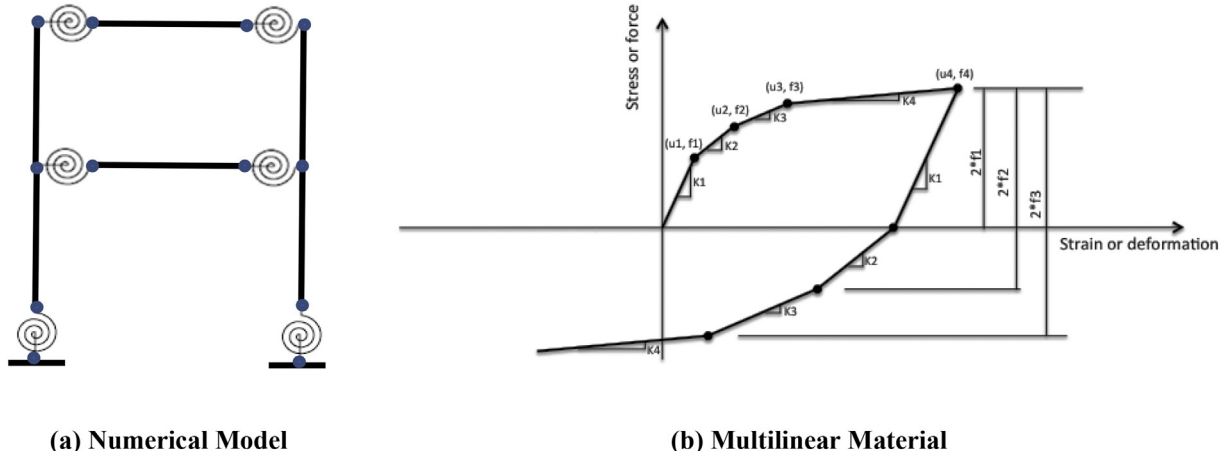


Fig. 21. Numerical Simulation.

sum of the bolt proof loads for the M12 Grade 8.8 structural bolts of 45kN, divided by the number of interfaces. This is equal to $42\text{kN}/(45\text{kN/bolt} \times 4\text{bolts} \times 1\text{interfaces}) = 0.23$. The friction coefficient for the base column connection (shown in the Fig. 6, north end, front frame) is slightly higher than for the beam end AFC (1st floor, front frame, north end, shown in the Fig. 6). The exact reason for this difference is not known and it may be due to differences in surface condition, construction sequence, and effect of magnitude of sliding displacement.

Also, because the beam and column maximum moment demands shown in Fig. 16 and Fig. 19 are less than the section plastic moment capacity ($M_h = F_y \times S = 24 \text{ kN.m}$), these elements remain essentially elastic.

6.2.5. Bolt tension force

The bolt tension obtained from the turn-of-the-nut method described previously was between 45 and 50 kN. Fig. 20 shows the tension force of the bolts during sliding under Bam, Christchurch (REHS), Northridge (Sylmar) and Kobe (KJM) ground motions ($\alpha_a=100\%$). It shows that bolt tension changed during sliding. However, when the plates returned back to their initial position, and the bolts became more vertical, the bolt tension force reduced as shown in Fig. 20 [4]. This is because bolt elongation occurs with bolts tightened to high tension forces where there is a high possibility of bolt yielding due to moment-shear-axial force interaction. Such a yielded bolt sustains permanent elongation and reduction in tension force, as observed in Fig. 20a and b. The maximum reduction in tension force after sliding was about 11% ($= 5\text{kN}/45\text{kN}$). This reduction occurred at drifts of 5.0% to 6.0% during the Bam and Christchurch (REHS) records with an acceleration scale of 100%. At lower drifts, of about 4%, such as that caused by the Northridge and Kobe records with acceleration scale of 100%, there was almost no residual reduction force in tension bolts as shown in Fig. 20.

7. Numerical simulation

The simple two-dimensional model shown in Fig. 21a was created using the software OpenSees [17] to simulating the nonlinear response under the earthquake excitations. The 2-D model was appropriate because torsional displacements of the frame were <0.1% of the peak values and could be ignored. A simple elastic element was used to model the elastically responding 100UC14.8, Grade 300 beams and columns. Zero-length elements were used to capture the friction connection moment-rotation behaviour. Lateral and vertical displacements of the both ends of the connections were constrained to the beams and columns. From modal analysis, the structure fundamental period was

0.46 s which is almost the same value as that obtained from the snap back test of 0.47 s as was described in Section 6.1.

7.1. Beam end connections

The AFC beam-end flexural behaviour was approximated by a trilinear model using the *MultiLinear Material* behaviour from OpenSees [17] as shown in Fig. 21b. The parameters were provided with following values based on the experimental results in Section 6.2.4. They were: Point (a) ($M = 3\text{kN.m}$, $\theta=0.01\%$); Point (b): ($M = 7\text{kN.m}$, $\theta=1.0\%$); and Point (c): ($M = 11\text{kN.m}$, $\theta=4.0\%$). As shown in Fig. 16, Point (a) describes when initial sliding occurs; Point (b) is when the second sliding occurs, and Point (c) is where the maximum positive rotation occurred. By specifying these three points in the forward direction loading, the model cyclic loading is also defined as shown in Fig. 21b.

7.2. Base column connection

A bilinear curve is used to approximate the AFC base column hysteretic behavior in Section 5.2. The OpenSees *Steel02 Material* (Giuffre-Menegotto-Pinto model, [18]) is used. Based on the experimental results, as shown in Fig. 19, the main parameters of the model were; (i) the initial sliding base column moment of 7kN.m ; (ii) a base column initial rotational stiffness of 30EI/L to represent rigid fixed base conditions [19], and (iii) a column post elastic stiffness of 7%. Moreover, the Giuffre-Menegotto-Pinto model [18] parameters controlling the transition from elastic to plastic branches were considered to be 18.5 for R_0 , 0.928 for cR_1 , and 0.15 for cR_2 [18].

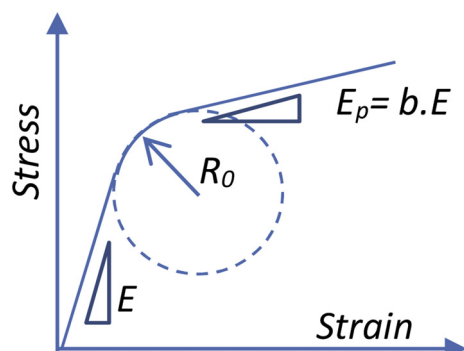


Fig. 22. The Giuffre-Menegotto-Pinto model.

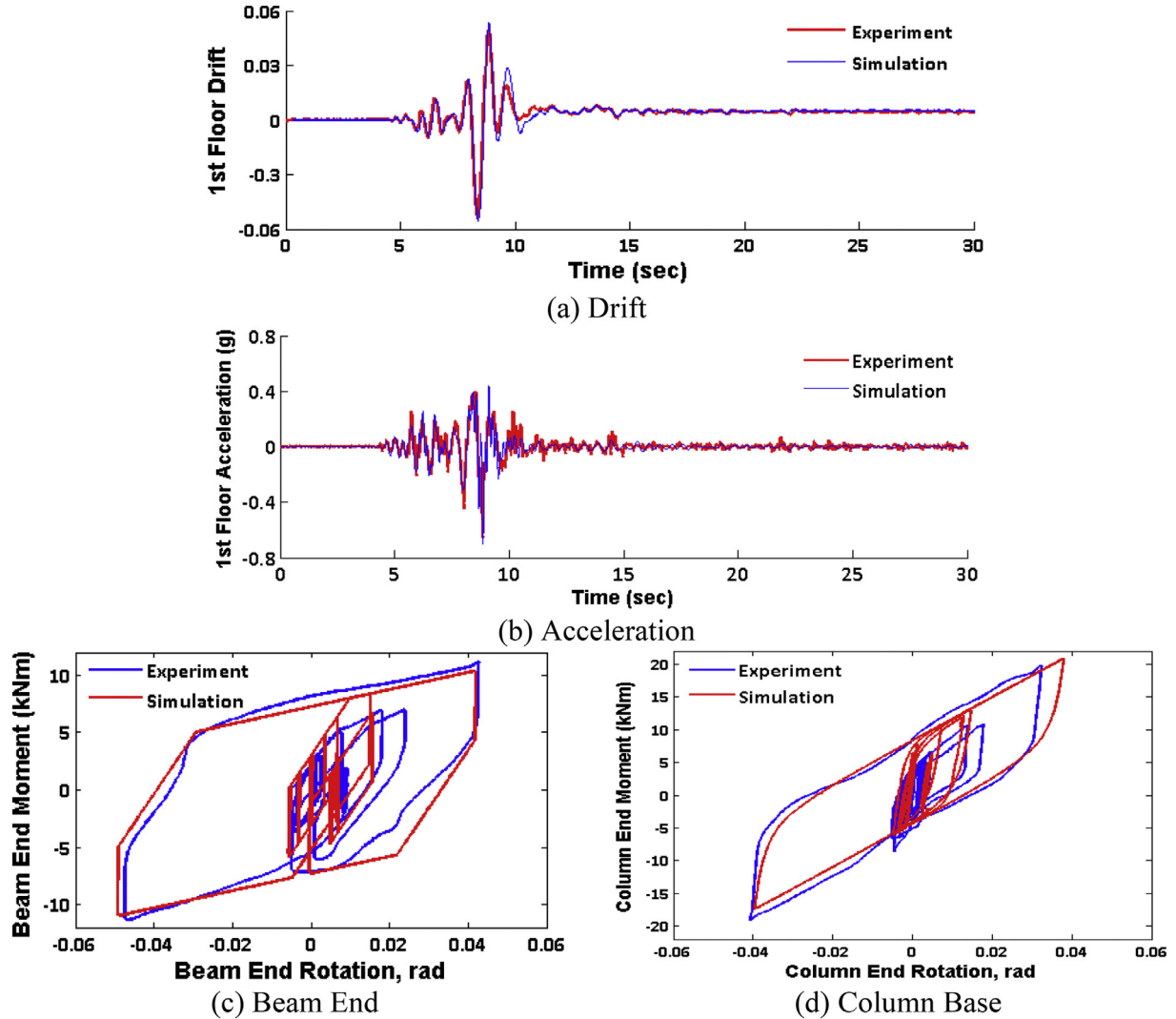


Fig. 23. Comparing experimental with numerical simulation under Christchurch (REHS) 2011 records ($ACC_{scale} = 100\%$).

7.3. Numerical simulation and experimental comparison

The numerical model was provided with initial mass proportional Rayleigh damping with a damping ratio of 3.4% (based on the test results) assigned to the first 2 modes of the structure. The ground motions used in the experimental study were applied to the numerical structural model.

Fig. 23 shows that the first level drift and acceleration time histories, and beam end and base column moment-rotation hysteresis curves, compared well with the test results. The simulated moments in the two final small cycles in **Fig. 22c** and d were higher than in the experiments. This may be due bolt tension force loss after big cycle of rotation in the joint. Which was not considered in the simulation. Since this does not have big effect on general response of the structure the simulation

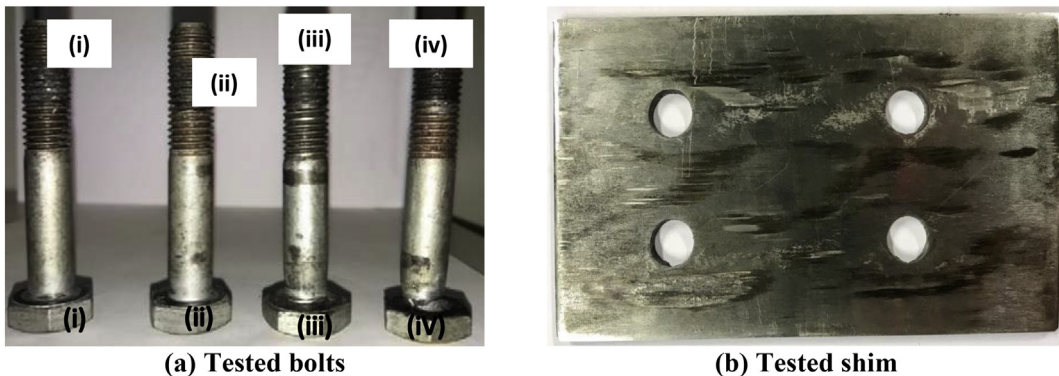


Fig. 24. SHJ bolt and shim damage after tests.

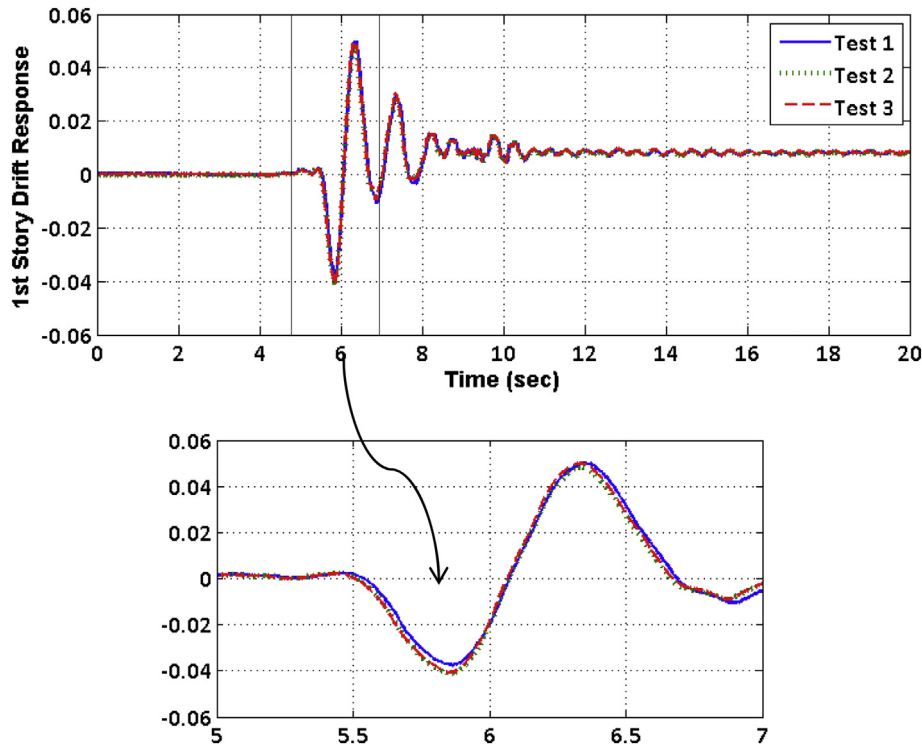


Fig. 25. Displacement response under repeatable shaking (Bam records, 100%).

seemed to capture key peak strength and deformation parameters characteristics.

Table 5 compares the simulated and experimental model peak and residual drifts for records with different acceleration scales. The most difference between the simulation and test was about 10%. Residual drifts <0.1% are reported as zero in the table. This value is less than normal frame out-of-straightness construction tolerances of 0.2% [13].

Sensitivity analyses were also undertaken understand the sensitivity of the friction coefficient parameter on the drift response. **Table 6** shows that by increasing friction coefficient by up to 20% the interstorey drift is decreased, but the amount of change was <5%.

8. Overall structural performance

From the ground motions considered, where peak drifts were up to 6%, there was no significant member damage. No column web or flange yielding or buckling was observed, and all flanges plates welded to the columns and base plates showed no sign of yielding or paint flaking. After very severe shaking, when there was bolt tension force reduction, new bolts were inserted and tightened before each run. **Fig. 24a** shows the condition of AFC bolts after different levels of shaking. Bolts (i) and (ii) underwent small inelastic cycles, so there is almost no shank damage. However, Bolts (iii) and (iv) underwent a significant number of large inelastic cycles which caused Bolt (iii) plastic deformation and Bolt (iv) fracture just below the bolt head. **Fig. 24b** also shows

Table 5
Peak and residual drift responses of simulated and experimental models.

No	Earthquake name	ACC _{scale}	Peak 1st floor drift		Peak 2nd floor drift		Residual 1st floor drift		Residual 2nd floor drift	
			Test	Simu	Test	Simu	Test	Simu	Test	Simu
1	Christchurch (CCCC)	50%	1.25%	1.1%	1.29%	1.15%	0	0	0	0
1	Christchurch (CCCC)	75%	2.39%	2.4%	2.63%	2.6%	0	0	0	0
1	Christchurch (CCCC)	100%	3.91%	4.0%	3.99%	4.1%	0.1%	0.12%	0.1%	0.13%
2	Bam, Iran	50%	1.9%	1.7%	2.03%	1.75%	0.17%	0.2%	0.19%	0.25
2	Bam, Iran	75%	3.3%	2.9%	3.5%	3.2%	0.27%	0.3%	0.29%	0.35%
2	Bam, Iran	100%	4.9%	4.7%	5.2%	4.8%	0.69%	0.65%	0.72%	0.7%
3	Northridge (Sylmar)	50%	0.89%	0.95%	0.96%	1.1%	0	0	0	0
3	Northridge (Sylmar)	75%	1.8%	1.65%	1.81%	1.8%	0	0	0	0
3	Northridge (Sylmar)	100%	2.93%	2.8%	3.21%	3.0%	0.11%	0.06%	0.11%	0.085%
4	Kobe (KJM), Japan	50%	2.38%	2.1%	2.62%	2.39%	0	0	0	0
4	Kobe (KJM), Japan	75%	3.2%	2.85%	3.6%	3.3%	0	0	0	0
4	Kobe (KJM), Japan	100%	3.6%	3.3%	4.35%	4.23%	0	0	0	0
5	Tabas, Iran	50%	1.47%	1.5%	1.7%	1.6%	0.1%	0.135%	0.12%	0.13%
5	Tabas, Iran	75%	2.4%	2.3%	2.6%	2.5%	0.12%	0.15%	0.16%	0.2%
5	Tabas, Iran	100%	3.7%	3.6%	3.9%	3.7%	0.18%	0.25%	0.24%	0.3%
6	Christchurch (REHS)	50%	2.63%	2.3%	2.71%	2.4%	0	0	0	0
6	Christchurch (REHS)	75%	4.0%	3.6%	4.6%	4.1%	0.18%	0.225%	0.2%	0.256%
6	Christchurch (REHS)	100%	5.5%	5.4%	6.1%	6.0%	0.47%	0.42%	0.54%	0.5%

Table 6

Sensitivity of friction coefficient on drift response (Christchurch, REHS, ACC_{scale} = 100%).

Friction coefficient increase (%)	1st story drift	2nd story drift	1st story diff. (%)	2nd story diff. (%)
0	5.4%	6.0%	–	–
5%	5.34%	5.90%	–1.11%	–1.67%
10%	5.25%	5.82%	–2.78%	–3.00%
15%	5.20%	5.76%	–3.70%	–4.00%
20%	5.17%	5.71%	–4.26%	–4.83%

an AFC shim after a number of inelastic cycles. The shims felt smooth with no gouging or visual damage.

Residual displacements were often small, especially when peak drifts were <2.5%. When there were residual displacements, usually from higher peak drifts, manual restraightening was carried out and the frame was brought back to its initial straight position. The structural performance was repeatable with peak and residual displacements errors <2.0% for straight structures subject to same record. This is shown for Bam ground motion in Fig. 25. For the reasons above, the overall structural performance of this structural system was considered to be excellent.

9. Conclusion

This paper describes seismic shake table tests of a half-scale two-storey steel building incorporating asymmetric friction connections (AFCs) at steel column bases and beam-column joints. Based on the experimental results obtained, the following conclusions can be drawn:

- 1) The hysteresis loop shapes for beam-column and base-column joints indicated tri-linear and bilinear characteristics respectively. Effective friction values, obtained when both surfaces started sliding, were 0.21 and 0.23 for beam ends and column bases respectively. These values were in the range of those recommended by MacRae et al. [4]. Moreover, there was almost no bolt tension force reduction after testing to frame drifts <4%. For cases with peak drifts of 6%, there was <10% strength reduction. It was also shown that prying, which is not included in previous beam end models, can be significant.
- 2) The structure peak displacement response was consistent with that from the ground motion spectral displacements. The structure moved approximately linearly with height. Also, the residual displacement was consistent with the residual displacement predictions.
- 3) A computational numerical model was developed and beam end moment rotation and peak displacements compared well with test results with a tolerance of about 10%.
- 4) The tests indicated no significant member damage even in drifts as high as 6%. The behaviour was repeatable and could be modelled with a tolerance of <2.0%. Residual displacements were generally

small, but reached 0.7% for peak drifts up to 6.0%. Even when there were residual displacements, manual restraightening allowed the structure to be fully repaired. Therefore, the structural system can be considered to be low-damage.

Acknowledgement

The authors would like to thank the University of Canterbury and the New Zealand Earthquake Commission (EQC) for providing financial support at various stages of the first author's PhD candidacy.

References

- [1] T.S. Yang, E.P. Popov, Experimental and Analytical Studies of Steel Connections and Energy Dissipators, Report No. UCB/EERC-95/13, Earthquake Engineering Research Centre, Berkeley, California, 1995.
- [2] G.C. Clifton, Development of perimeter moment-resisting steel frames incorporating semi-rigid elastic joints, N. Z. Natl. Soc. Earthq. Eng. Conf. (1996) 177–184.
- [3] G.C. Clifton, Semi-Rigid Joints for Moment-Resisting Steel Framed Seismic-Resisting Systems, PhD Thesis Department of Civil and Environmental Engineering, University of Auckland, 2005.
- [4] G.A. MacRae, G.C. Clifton, H. Mackinven, N. Mago, J. Butterworth, S. Pampanin, The sliding hinge joint moment connection, NZSEE Bull. 43 (3) (2010) 202–212.
- [5] J. Borzouie, G.A. MacRae, J.G. Chase, G.W. Rodgers, G.C. Clifton, Experimental studies on cyclic performance of column base strong axis-aligned asymmetric friction connections, J. Struct. Eng., 2015, [https://doi.org/10.1061/\(ASCE\)ST.1943-541X.0001327](https://doi.org/10.1061/(ASCE)ST.1943-541X.0001327).
- [6] J.C. Chanchí, G.A. MacRae, J.G. Chase, G.W. Rodgers, C.G. Clifton, Behaviour of Asymmetrical Friction Connections Using Different Shim Materials, NZSEE Conf, New Zealand Society for Earthquake Engineering, Wellington, New Zealand, 2012.
- [7] J.C. Chanchí, R. Xie, G. MacRae, G. Chase, G. Rodgers, C. Clifton, Low-Damage Braces Using Asymmetrical Friction Connections (AFC), NZSEE Conf, The New Zealand Society for Earthquake Engineering, Auckland, New Zealand, 2014.
- [8] J. Borzouie, G.A. MacRae, J.G. Chase, G.W. Rodgers, G.C. Clifton, Experimental studies on cyclic performance of column base weak axis aligned asymmetric friction connection, J. Constr. Steel Res. 112 (2015) 252–262.
- [9] G.A. MacRae, K. Kawashima, Post-earthquake residual displacements of bilinear oscillators, Earthq. Eng. Struct. Dyn. 26 (1997) 701–716.
- [10] G.A. MacRae, Y. Kimura, C.W. Roeder, Effect of column stiffness on braced frame seismic behavior, J. Struct. Eng. ASCE. March 130 (3) (2004) 381–391.
- [11] NZS 1170.5, Structural Design Actions Part 5: Earthquake Actions New Zealand. Standards New Zealand: Wellington, New Zealand, 2016.
- [12] G.A. MacRae, G.C. Clifton, Research on seismic performance of steel structures, Steel Innovations 2015 Conference Auckland, 2015.
- [13] NZS3404, Steel Structures Standard, Standards New Zealand, Wellington, New Zealand, 2007.
- [14] H.H. Khoo, C. Seal, G.C. Clifton, J. Butterworth, G.A. MacRae, Behaviour of top and bottom flange plates in the sliding hinge joint, Bull. NZ Soc. Earthq. Eng. 46 (1) (March 2013) 1–10 (ISSN No. 1174–9857).
- [15] B.A. Bradley, M. Cubrinovski, Near-source strong ground motions observed in the 22 February 2011 Christchurch earthquake, Seismol. Res. Lett. 82 (6) (2011) 853–865.
- [16] K.W. Campbell, Y. Bozorgnia, NGA ground motion model for the geometric horizontal component of PGA, PGV, PGD and 5% damped linear elastic response spectra for periods ranging from 0.01 to 10s, Earthquake Spectra 24 (1) (2008) 139–171.
- [17] OpenSees, Open System for Earthquake Engineering Simulation-Home Page, <http://opensees.berkeley.edu> 2017.
- [18] M. Menegotto, P.E. Pinto, Methods of analysis of cyclically loaded RC plane frames including changes in geometry and non-elastic behaviour of elements under normal force and bending, Prelim. Rep. IABSE (1973) 13.
- [19] Eurocode 3, Design of Steel Structures, British Standard, 2005.